ACS Macro Letters

Letter

pubs.acs.org/macroletters

Antitumor Efficacy of Irreversible Electroporation and Doxorubicin-Loaded Polymeric Micelles

Jun Zhao,[†] Yang Qiao,[‡] Min Zhou,[†] Michael Wallace,[‡] Sanjay Gupta,[‡] Chun Li,*[,†] and Marites P. Melancon*[,‡]

[†]Department of Cancer Systems Imaging and [‡]Department of Interventional Radiology, The University of Texas MD Anderson Cancer Center, Houston, Texas 77030, United States

Supporting Information

ABSTRACT: Irreversible electroporation (IRE), a nonthermal ablative treatment for unresectable tumors, applies an electrical field across the cell membrane, creating irreparable pores. Compared with conventional thermal ablation, IRE can preserve nearby structures. However, tumors may recur in regions exposed to insufficient electrical field strength. We developed a novel doxorubicin-loaded polymeric micelle system (M-Dox) using oil-in-water emulsion. M-Dox particles were 37.9 nm ± 3.2 nm in diameter, with 4.3% Dox loading by weight. M-Dox was toxic to four human cancer cell lines at nanomolar and micromolar median inhibitory concentrations. We used a hepatic carcinoma xenograft mouse model to evaluate the antitumor efficacy of M-Dox and IRE. Tumors treated with IRE + M-Dox had the highest M-Dox uptake and percentage of necrotic cells, compared with the monotherapy and control groups. Immunohistochemical staining confirmed that the combination group had the fewest proliferating cells. Our data suggest that adjuvant M-Dox enhanced the antitumor efficacy of IRE.

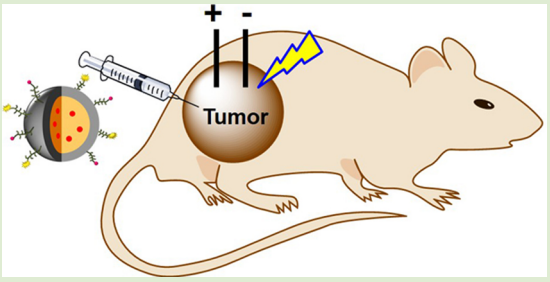

For patients with unresectable tumors, minimally invasive therapies are important alternatives to ablate tumors locally.[1] Most ablative techniques kill tumor cells by inducing significant temperature change within the ablation zone.[2] However, treatment response is often complicated by collateral damage to nearby ducts or blood vessels. The efficacy of thermal ablation also can be limited by the "heat sink" effect, in which the blood flow in the adjacent vasculature dissipates the thermal energy and causes suboptimal ablation and eventually tumor recurrence.[3] Irreversible electroporation (IRE) has proven useful in treating patients with perivascular tumors.[4] Unlike thermal ablation, IRE selectively disrupts cell membranes by creating irreparable pores and enables the intracellular delivery of nanoparticles.[5] The persistent leakage of the cell membrane soon leads to the loss of endocytic homeostasis and consequent cell death.[6] IRE has many advantages over conventional thermal ablation. IRE affects only cell membranes, sparing most of the other cellular components or nearby tissues. The treatment can be administered relatively quickly, over several minutes.[7] Importantly, IRE preserves nearby sensitive structures (e.g., the urethra and myelin sheaths)[8] and leaves the extracellular matrix and major tissue vasculature largely intact. IRE usually causes a minimal scar that heals several weeks after treatment. The rapidly absorbed scar will not interfere with the post-treatment diagnosis of residual or recurrent tumors.[9]

The cell-killing efficacy of IRE depends on the strength of the local electrical field. If the cell membrane is able to recover following the electrical pulses, the effect is called reversible electroporation (RE). Although RE has been used extensively to transport molecules or nanoparticles across the cell membrane,[10] RE does not kill tumor cells by itself. Tumor cells exposed to insufficient electrical field strength may survive, resulting in tumor recurrence. The number of residual tumor cells can be minimized by using IRE probes with advanced array geometry along with mathematical simulation of the distribution of the intratumoral electrical field strength.[11] However, owing to the irregular geometry and heterogeneity of tumor masses, it is difficult to achieve uniform IRE-induced necrosis throughout the tumor mass.

Chemotherapy drugs, such as bleomycin,[12] have been used to boost the antitumor efficacy of RE. To determine whether chemotherapy drugs also can augment the antitumor effects of IRE, we developed a novel doxorubicin-loaded micelle system (M-Dox) and evaluated its antitumor efficacy in combination with IRE. We hypothesized that the combination of IRE and M-Dox would have better antitumor efficacy than IRE alone.

M-Dox was prepared via oil-in-water emulsion using a cross-linkable block copolymer as the macromolecular surfactant (Figure 1A). The proton nuclear magnetic resonance (^{1}H NMR) spectrum revealed that each copolymer was constituted of 10 units of methoxy-PEG-methacrylate (MAPEG, hydrophilic block) and 20 units of 2-(methacryloyloxy)ethyl 4-oxo-4-(3-(triethoxysilyl)propylamine)butanoate (MESPS, hydropho-

Received: August 4, 2015
Accepted: September 9, 2015
Published: September 11, 2015

DOI: 10.1021/acsmacrolett.5b00545
ACS Macro Lett. 2015, 4, 1081−1084

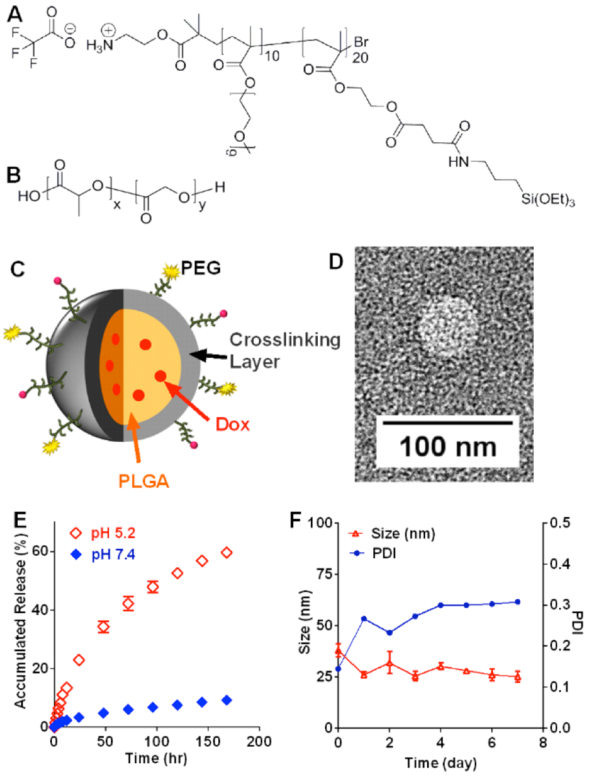

Figure 1. Preparation and characterization of doxorubicin-loaded micelles (M-Dox). Chemical structure of cross-linkable block copolymer (A) and poly(lactic-*co*-glycolic acid) (PLGA) (B). (C) Schematic illustration of M-Dox particle. PLGA (yellow), Dox (red), cross-linking layer (gray). (D) Transmission electron microscopy micrograph of M-Dox particles (scale bar = 100 nm). (E) Doxorubicin release profile at 37 °C. (F) Hydrodynamic size and polydispersity index (PDI) of M-Dox particles during degradation at 37 °C.

bic block). The oil phase contained the biodegradable poly(lactic-*co*-glycolic acid) (PLGA, Figure 1B) and doxorubicin. The resultant M-Dox particles (Figure 1C) were 37.9 nm ± 3.2 nm in diameter (polydispersity index [PDI], 0.145), with 4.3% Dox loading by weight. Transmission electron microscopy (TEM) confirmed that the M-Dox particle had a spherical morphology with diameters around 50 nm (Figure 1D).

Owing to the acid-induced degradation of PLGA, Dox was released from M-Dox at 37 °C in a pH-dependent manner (Figure 1E). The release of Dox was faster at pH 5.2 than at pH 7.4. Up to 60% of Dox was released at pH 5.2 after 7 days of incubation, at which time less than 10% was released at pH 7.4. Notably, the size of the M-Dox particles did not change dramatically during degradation, probably because of the cross-linking silane. After 7 days of incubation at 37 °C, the particle size decreased from 37.9 nm ± 3.2 to 25.2 nm ± 2.5 nm. The PDI increased from 0.145 to 0.308 (Figure 1F), suggesting that partial degradation may have occurred.

We first studied the effect of M-Dox on cell viability in four cancer cell lines (Figure S1): U87 (human glioblastoma), HeLa (human cervical cancer), MIA PaCa-2 (human pancreatic adenocarcinoma), and Hep3B (human hepatocellular carcinoma). Cell viability was measured after 96 h of incubation with conventional Dox or M-Dox. Both Dox and M-Dox showed excellent antiproliferation efficacy, although M-Dox was less cytotoxic than Dox. The antiproliferation median inhibitory concentration values for Dox and M-Dox (nM) were 77.5 ± 8.9 vs 444.9 ± 33.5 for U87, 17.1 ± 2.5 vs 51.8 ± 6.1 for HeLa, 0.97 ± 0.07 vs 30.7 ± 2.6 for MIA PaCa-2, and 30.5 ± 2.5 vs 92.1 ± 8.0 for Hep3B.

We then tested the effect of electroporation field strength (V/cm) on Hep3B cell viability (Figure 2A). We did not

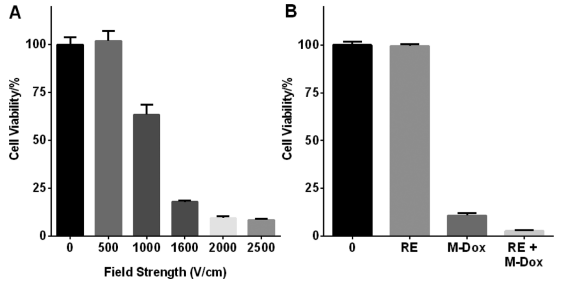

Figure 2. Effect of doxorubicin-loaded micelles (M-Dox) and electroporation treatment on Hep3B cell viability. (A) Hep3B cell viability after electroporation at different field strengths. (B) Hep3B cell viability in untreated cells and in cells treated with M-Dox alone, reversible electroporation (RE, 500 V/cm) alone, and RE + M-Dox. The combination group had the fewest viable cells of all four groups ($p < 0.05$).

observe significant cell death at field strengths up to 500 V/cm; above this threshold, cell viability decreased as the field strength increased. Therefore, we defined the field strength of RE as 500 V/cm and of IRE as 2500 V/cm. For *in vitro* combination therapy, Hep3B cells were treated with M-Dox (50 μM) and RE. Untreated cells and monotherapy groups were used as controls. Figure 2B shows that the combination group had significantly fewer viable cells than the monotherapy groups ($p < 0.05$). Blank micelles did not have a significant impact on cell viability (Figure S3).

We used a Hep3B subcutaneous xenograft mouse model to investigate the *in vivo* effects of combination therapy. Tumors were collected 24 h after treatment and sectioned for the analysis of M-Dox uptake, necrosis, and cell proliferation. Figure 3 summarizes the M-Dox uptake results. Compared with M-Dox monotherapy, both RE + M-Dox and IRE + M-Dox increased the number of M-Dox-positive nuclei, by 1.7 and 2.7 times, respectively ($p < 0.05$). Figure 4 shows representative

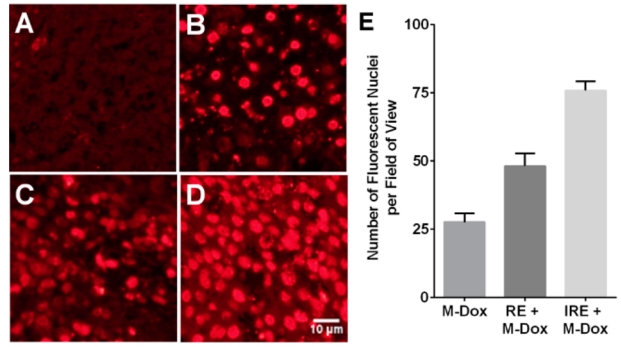

Figure 3. *In vivo* uptake of doxorubicin-loaded micelles (M-Dox) in the presence of electroporation. (A) Untreated control, (B) M-Dox, (C) reversible electroporation (RE) + M-Dox, (D) irreversible electroporation (IRE) + M-Dox. The quantitative results are summarized in panel E. Data points are presented as means ± standard error of mean ($N = 9$). Each group was significantly different from each other ($p < 0.05$).

DOI: 10.1021/acsmacrolett.5b00545
ACS Macro Lett. 2015, 4, 1081−1084

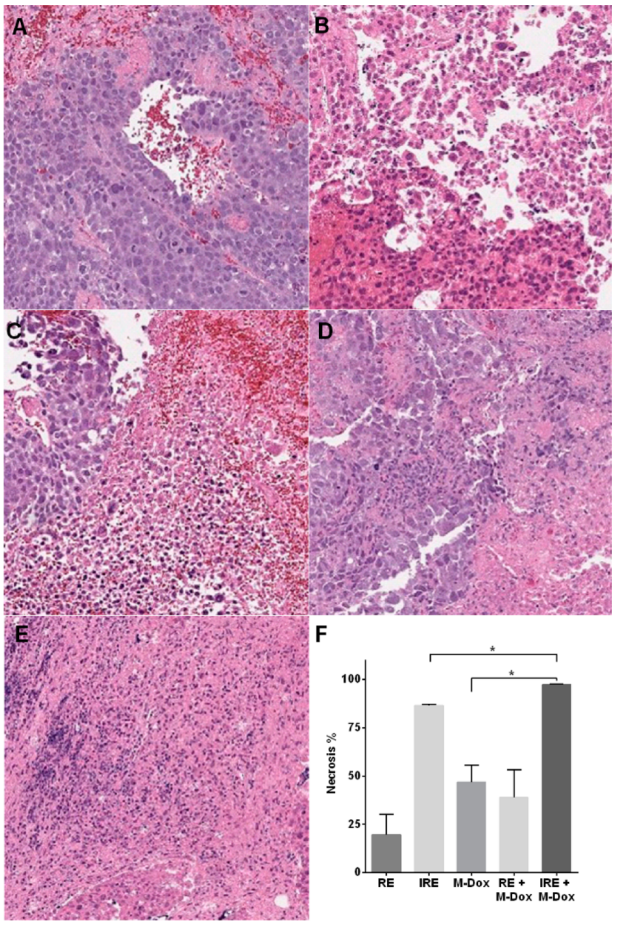

Figure 4. Hematoxylin and eosin analysis of treated tumors and quantification of necrotic cells. (A) Reversible electroporation (RE), (B) irreversible electroporation (IRE), (C) doxorubicin-loaded micelles (M-Dox), (D) RE + M-Dox, and (E) IRE + M-Dox. The quantitative results are summarized in panel F. Data points are presented as means ± standard error of mean (N = 3).

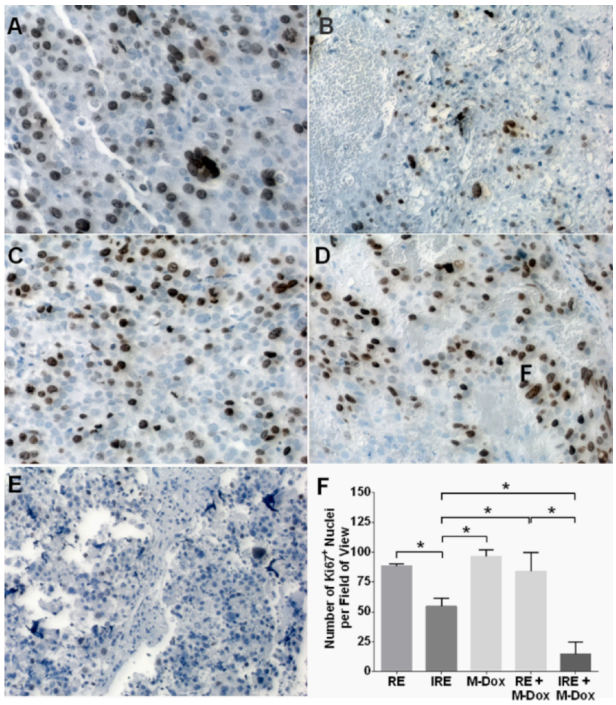

Figure 5. Immunohistochemical staining for proliferating cells (Ki67+) on sections of treated tumors. Representative micrographs are shown in panels A–E: (A) reversible electroporation (RE), (B) irreversible electroporation (IRE), (C) doxorubicin-loaded micelles (M-Dox), (D) RE + M-Dox, and (E) IRE + M-Dox. The quantitative results are summarized in panel F. Data were generated from at least 10 randomly chosen field of views in each treatment group. Significant differences are marked with * (p < 0.05).

tumor necrosis from tumor tissue stained with hematoxylin and eosin. The percentage of necrotic cells in IRE + M-Dox-treated tumors (97.2 ± 0.5%) was significantly higher than those of tumors treated with IRE alone (86.5 ± 0.5%) or M-Dox alone (46.7 ± 9.1%) (p < 0.05). Figure 5 shows the cell proliferation of treated tumors. Of the monotherapy groups, the IRE group had fewer proliferating cells than the RE or M-Dox groups (p < 0.05). The IRE + M-Dox group had fewer proliferating cells than the IRE or M-Dox groups (p < 0.05).

In this study, we developed a novel M-Dox system using an *in situ* cross-linkable amphiphilic polymeric stabilizer. The M-Dox particles had excellent cytotoxicity in four types of human cancer cells. The combination of IRE and M-Dox showed better antitumor efficacy in a Hep3B xenograft model than the monotherapy groups.

Oil-in-water emulsion is widely used to prepare nanoparticles loaded with hydrophobic chemotherapy drugs.[13] An important step during the emulsion is to form a stable dispersion of micrometric oil droplets stabilized by small-molecular or macromolecular surfactants.[13] During the postemulsion evaporation, the organic solvent inside the oil droplets evaporates, and the microdroplets solidify into nanoparticles coated by the surfactants. However, since most surfactants are not covalently bound to the nanoparticles, the stability of the nanoparticles may be insufficient. Hydrolytically cross-linkable polymers have been synthesized via various methods.[14] We hereby developed a novel amphiphilic polymeric surfactant, PEG-*b*-poly(MESPS), which can cross-link *in situ* through the hydrolysis of silane groups. As a result, the PLGA/Dox cores were covered by a mesh network of cross-linked PEG-*b*-poly(MESPS) (Figure 1C). Notably, the silane group was linked to the polymer backbone via a biodegradable succinic monoester bond.[15] Therefore, the cross-linking unit can shed from the micelles over time. The ammonium functionality at the exterior termini of the PEG block (Figure 1A) also could be used to conjugate with targeting ligands or diagnostic imaging tracers.[16] Owing to the cross-linked silane, M-Dox showed excellent size stability (Figure 1F) and retained most of the Dox up to 1 week at physiological pH (Figure 1E). Dox was released in an acidic environment, which is advantageous since tumor microenvironments typically are acidic.[17] The antitumor efficacy of M-Dox was validated in four human cancer cell lines, with nanomolar or micromolar median inhibitory concentration values (Figure S1). M-Dox was less cytotoxic than Dox probably because of the controlled release of the drug in M-Dox during incubation.

To our best knowledge, M-Dox is the first polymeric nanoformulation that has been used in combination with IRE to demonstrate treatment efficacy. Mouli et al.[18] recently published on the use of superparamagnetic iron oxide nanoparticles loaded with doxorubicin in combination with IRE to increase the accumulation of drug-carrying nanoparticles in N1S1 rat hepatoma and VX2 rabbit tumor models. Although the authors showed increased accumulation of the nanoparticles in the target tissues, treatment efficacy was not presented. As

DOI: 10.1021/acsmacrolett.5b00545
ACS Macro Lett. 2015, 4, 1081–1084

shown in Figure 3, more cell nuclei expressed the fluorescence of Dox after IRE or RE than in the control group. M-Dox was directly injected into tumors so that each tumor was exposed to the same dose of M-Dox. Without electroporation, the intratumoral distribution of M-Dox was uneven (Figure 3B); this finding supports previous reports of the limitations of intratumoral injection. Electroporation increased the intracellular delivery of M-Dox: IRE was more potent than RE (Figure 3D vs Figure 3C) probably because IRE could better permeate cell membranes.

For our antitumor efficacy studies, we found *in vitro* that the combination group (RE + M-Dox) had fewer viable cells than the groups treated with RE alone or M-Dox alone (Figure 2B), indicating that M-Dox could enhanced the antitumor efficacy within the reversible zone. We further evaluated the antitumor efficacy of M-Dox in combination with electroporation in a Hep3B xenograft model. Treating tumors with electroporation and M-Dox caused acute tumor necrosis (Figure 4). Of all the treatment groups, IRE + M-Dox caused the highest percentage of necrotic cells. The necrosis data correlated with the immunohistochemical staining results for cell proliferation (Figure 5), in which the IRE + M-Dox-treated tumor tissue had the fewest proliferating cells ($Ki67^+$) of all experimental groups.

Our study had several limitations. We analyzed only acute tumor response, and the M-Dox particles were intratumorally injected. Long-term monitoring of tumor growth and animal survival is necessary to understand the antitumor efficacy of this combination therapy. To improve the intratumoral distribution of nanoparticles, we will use intravenous injection of M-Dox in future studies. The uptake of M-Dox in tumors and other organs will be determined by a biodistribution study.

In summary, we developed a novel doxorubicin-loaded micelles via oil-in-water emulsion technique. Our results showed that combining electroporation and M-Dox effectively inhibited four cultured cell lines and a human hepatic carcinoma xenograft model. While IRE treatment killed most tumor cells, adjuvant M-Dox treatment further increased the percentage of necrotic cells and decreased the proliferating tumor cells. Further studies are warranted to evaluate survival of animals treated with systemic drug-loaded nanoparticles.

■ ASSOCIATED CONTENT

Supporting Information

The Supporting Information is available free of charge on the ACS Publications website at DOI: 10.1021/acsmacrolett.5b00545.

Detailed experimental procedures (PDF)

■ AUTHOR INFORMATION

Corresponding Authors

*E-mail: mmelancon@mdanderson.org.

*E-mail: cli@mdanderson.org.

Notes

The authors declare no competing financial interest.

■ ACKNOWLEDGMENTS

This work was supported in part by the John S. Dunn Foundation. The High Resolution Electron Microscopy Facility, Nuclear Magnetic Resonance Facility, and the Research Animal Support Facility were supported by a Cancer Center Support Grant from the National Institutes of Health (P30CA016672). The funding sources were not involved in study design; in the collection, analysis, and interpretation of data; in the writing of the report; or in the decision to submit the article for publication. We thank Stephanie Deming for editing the manuscript.

■ REFERENCES

(1) Wyld, L.; Audisio, R. A.; Poston, G. J. *Nat. Rev. Clin. Oncol.* **2015**, *12* (2), 115−124.

(2) Li, D.; Kang, J.; Golas, B. J.; Yeung, V. W.; Madoff, D. C. *Cancer Biol. Med.* **2014**, *11* (4), 217−236.

(3) Mulier, S.; Ni, Y.; Jamart, J.; Ruers, T.; Marchal, G.; Michel, L. *Ann. Surg.* **2005**, *242* (2), 158−71.

(4) Charpentier, K. P.; Wolf, F.; Noble, L.; Winn, B.; Resnick, M.; Dupuy, D. E. *HPB (Oxford)* **2011**, *13* (3), 168−173.

(5) (a) Davalos, R. V.; Mir, I. L.; Rubinsky, B. *Ann. Biomed. Eng.* **2005**, *33* (2), 223−31. (b) Jaroszeski, M. J.; Coppola, D.; Nesmith, G.; Pottinger, C.; Hyacinthe, M.; Benson, K.; Gilbert, R.; Heller, R. *Eur. J. Cancer* **2001**, *37* (3), 414−21.

(6) Guo, Y.; Zhang, Y.; Klein, R.; Nijm, G. M.; Sahakian, A. V.; Omary, R. A.; Yang, G.-Y.; Larson, A. C. *Cancer Res.* **2010**, *70* (4), 1555−1563.

(7) Cannon, R.; Ellis, S.; Hayes, D.; Narayanan, G.; Martin, R. C., 2nd *J. Surg. Oncol.* **2013**, *107*, 544.

(8) Neal, R. E.; Davalos, R. V. *Ann. Biomed. Eng.* **2009**, *37* (12), 2615−2625.

(9) Rubinsky, B.; Onik, G.; Mikus, P. *Technol. Cancer Res. Treat.* **2007**, *6* (1), 37−48.

(10) (a) Yamashita, Y. I.; Shimada, M.; Hasegawa, H.; Minagawa, R.; Rikimaru, T.; Hamatsu, T.; Tanaka, S.; Shirabe, K.; Miyazaki, J. I.; Sugimachi, K. *Cancer Res.* **2001**, *61* (3), 1005−1012. (b) Granot, Y.; Rubinsky, B. *Int. J. Heat Mass Transfer* **2008**, *51* (23−24), 5610−5616.

(11) (a) Arena, C. B.; Sano, M. B.; Rylander, M. N.; Davalos, R. V. *IEEE Trans. Biomed. Eng.* **2011**, *58* (5), 1474−82. (b) Gowrishankar, T. R.; Esser, A. T.; Smith, K. C.; Son, R. S.; Weaver, J. C. *Conf Proc. IEEE Eng. Med. Biol. Soc.* **2011**, *2011*, 732−5.

(12) Jaroszeski, M. J.; Gilbert, R. A.; Heller, R. *Biochim. Biophys. Acta, Gen. Subj.* **1997**, *1334* (1), 15−8.

(13) Choudhury, H.; Gorain, B.; Karmakar, S.; Biswas, E.; Dey, G.; Barik, R.; Mandal, M.; Pal, T. K. *Int. J. Pharm.* **2014**, *460* (1−2), 131−43.

(14) (a) Du, J.; Armes, S. P. *J. Am. Chem. Soc.* **2005**, *127* (37), 12800−1. (b) Zhu, W.; Li, Y.; Liu, L.; Zhang, W.; Chen, Y.; Xi, F. *J. Biomed. Mater. Res., Part A* **2011**, *96* (2), 330−340.

(15) Zhao, J.; Song, S.; Zhong, M.; Li, C. *ACS Macro Lett.* **2012**, *1* (1), 150−153.

(16) Tadros, T.; Izquierdo, P.; Esquena, J.; Solans, C. *Adv. Colloid Interface Sci.* **2004**, *108−109*, 303−18.

(17) Wang, L.; Fan, Z.; Zhang, J.; Changyi, Y.; Huang, C.; Gu, Y.; Xu, Z.; Tang, Z.; Lu, W.; Wei, X.; Li, C. *Int. J. Cancer* **2015**, *136* (4), E107−16.

(18) Mouli, S. K.; Tyler, P.; McDevitt, J. L.; Eifler, A. C.; Guo, Y.; Nicolai, J.; Lewandowski, R. J.; Li, W.; Procissi, D.; Ryu, R. K.; Wang, Y. A.; Salem, R.; Larson, A. C.; Omary, R. A. *ACS Nano* **2013**, *7* (9), 7724−33.

DOI: 10.1021/acsmacrolett.5b00545
ACS Macro Lett. 2015, 4, 1081−1084